Desalination and Water Treatment
www.deswater.com

doi: 10.5004/dwt.2021.26618

212 (2021) 311–322
February

A novel magnetically separable $CoFe_2O_4/SnO_2$ composite photocatalyst for the degradation of methylene blue dye from aqueous solution

Md. Tamez Uddin, Muhammad Zobayer Bin Mukhlish*, Md. Rifat Hossain Patwary

Department of Chemical Engineering and Polymer Science, Shahjalal University of Science and Technology, Sylhet 3114, Bangladesh, Tel. +8801912815531; emails: zobayer_ceps@yahoo.com/zobayer-cep@sust.edu (M.Z.B. Mukhlish), mtuddin_cep@yahoo.com (Md. Tamez Uddin), rifat.sust.cep13@gmail.com (Md. Rifat Hossain Patwary)

Received 27 April 2020; Accepted 30 September 2020

ABSTRACT

In this paper, a magnetically separable $CoFe_2O_4/SnO_2$ nanocomposite was synthesized by a two-step procedure, first, the synthesis of $CoFe_2O_4$ and SnO_2 nanoparticles by wet chemical precipitation method and second, the preparation of $CoFe_2O_4/SnO_2$ nanocomposites by solid-state reaction method. The resulting photocatalysts were characterized by X-ray diffraction (XRD), nitrogen adsorption–desorption analyses, scanning electron microscopy, energy dispersive X-ray spectroscopy (EDX) and UV-vis diffuse reflectance spectroscopy. The crystallization investigated by XRD confirmed the existence of both SnO_2 and $CoFe_2O_4$ phases, which was further confirmed by EDX. The energy band gap of 5% $CoFe_2O_4/SnO_2$ nanocomposite observed by UV-Vis diffuse reflectance spectroscopy was estimated to be 3.7 eV, which was comparable with that of SnO_2. The photocatalytic performance of the as-synthesized magnetic $CoFe_2O_4/SnO_2$ nanocomposites was investigated through methylene blue degradation reaction under UV irradiation. The $CoFe_2O_4/SnO_2$ nanocomposite containing 5 wt.% $CoFe_2O_4$ exhibited improved photocatalytic performance compared with commercial P-25. Moreover, alkaline media was favorable for photocatalytic degradation of cationic dye methylene blue. Finally, $CoFe_2O_4/SnO_2$ nanoparticles can be separated and recovered quickly from suspension in the presence of an externally applied magnetic field without leaving residues in the solution. Therefore, it can be concluded that this work would replace the traditional semiconductor photocatalysts and the as-synthesized photocatalyst would be a promising candidate for environmental cleanup.

Keywords: $CoFe_2O_4/SnO_2$; Magnetic photocatalyst; Complete mineralization; Methylene blue

1. Introduction

Synthetic dyes are widely used as coloring agents in various industries including textiles, leather, printing, and paper. These industries generate a large volume of dye-contaminated wastewater. The presence of dyes in the effluents is of great concern from the environmental viewpoint because dyes tend to suppress photosynthetic activity in aquatic habitats by preventing the penetration of sunlight [1] that leads to reduced dissolved oxygen levels affecting the entire aquatic biota [2]. Besides, synthetic azo dyes are identified as carcinogenic and mutagenic compounds and cause a potential threat to aquatic organisms as well as human life [3–7]. Furthermore, textile wastewater containing azo dyes is often used, in developing countries, to irrigate crops, which adds harmful azo dyes to agricultural soils. These azo compounds are very negative to soil microbial communities and to germination and growth of plants [1]. Therefore, the treatment of effluent containing such dyes is of grave concern to ensure the sustainability of the environment to future generations.

The most currently used physicochemical and biological treatment methods, which include adsorption,

* Corresponding author.

coagulation–flocculation, and activated sludge processes, fail to completely destroy dye pollutants, and are also slow, require expensive equipment, and can lead to secondary pollution [8–10]. In recent years, advanced oxidation processes (AOPs) have been proved to be promising techniques for complete degradation of organic pollutants in aqueous environment [11]. Among AOPs, the semiconductor heterogeneous photocatalysis has recently been investigated and evaluated as an alternative economical and harmless technology for total mineralization of toxic organic pollutants to H_2O and CO_2 as end products [12–17].

Over the past decades, semiconductor metal oxide nanoparticles such as WO_3, TiO_2, ZnO, Fe_2O_3, ZrO_2, CuO, CdS, ZnS and SnO_2 have drawn increasing attention as photocatalysts owing to their higher surface areas and much more surface active sites than bulk materials [17–20]. Tin oxide (SnO_2) is an important *n*-type semiconductor material and has been used in many fields including gas sensors [21], solar cells [22,23], transparent conducting electrodes [24], conductive filler [25], adsorption [26], biomedical [27], photocatalysis [28,29] and so on. SnO_2 has a wide band gap of 3.7 eV at room temperature with excellent optical and electrical properties [26]. Moreover, SnO_2 possesses high electron mobility (~100 to 200 $cm^2\ V^{-1}\ s^{-1}$), indicating a faster transport of photoexcited electrons. The structure, band gap and chemical stability of SnO_2 are similar to those of titanium dioxide (TiO_2), which is a widely used photocatalyst [8]. Crystal structure and particle size are considered as important factors that determine photoactivity. It is reported that photocatalytic reaction efficiency can be affected by the number of absorbed photons by photocatalysts surface, which indicates that the photocatalytic reaction takes place on the adsorbed surface [30]. Thus, the high degradation efficiency is obtained with the photocatalyst with high surface area, which results from small particle size. On the other hand, the preparation of small spherical photocatalyst particles with high crystallinity is critical because such particles have high stability and large surface area in aqueous solution [31]. The widely used semiconductors such as TiO_2, ZnO and WO_3 are easily aggregated during heat treatment resulting in large particle size and hence small surface area. In addition, ZnO can be easily dissolved in both acidic and alkaline solution due to its amphoteric properties. This dissolution of ZnO is further accelerated under UV light irradiation [32]. Thus, zinc oxide exhibits relatively low chemical stability due to the light-induced photocorrosion. In contrast, SnO_2 is highly stable in aqueous medium even under UV light irradiation and have high surface area [33]. In our previous study, SnO_2 nanoparticles with high specific area (90 m^2/g) were prepared by homogeneous precipitation method [34]. Thus, SnO_2 exhibits superior physical and chemical properties than other semiconductor metal oxides. The potential use of SnO_2 in photocatalytic degradation of organic pollutants has particularly aroused great interest due to its low cost, high specific area, chemical stability, nontoxic nature and remarkable adsorption capacity [8,35].

Although the SnO_2 nanoparticles exhibit high photocatalytic activity [17,36], the nanoparticles are impractical for industrial applications because the photocatalyst nanoparticles are mostly used as slurry in a photoreactor and the separation and recovery of slurry nanoparticle photocatalysts from wastewater can be costly and technically difficult to perform due to their small particle size. In addition, suspended nanoparticles are easily lost in the process of photocatalytic reaction and separation or discharged to the environment, which may cause secondary pollution problem [37]. In order to overcome this problem, developing nanoparticles with easy solid–liquid separation property without harming its photocatalytic performance has become very important. One important approach is to develop magnetic photocatalyst that allows easy separation of catalyst by using an external magnet, simplifying the downstream recovery stage. $CoFe_2O_4$ nanoparticle, a typical ferromagnetic oxide and low band gap semiconductor, is well known to have large magnetic anisotropy, moderate saturation magnetization, remarkable chemical stability and mechanical hardness [38]. In addition, $CoFe_2O_4$ has superior magnetic properties than CoO or Fe_3O_4 alone, which implies that $CoFe_2O_4$ nanoparticles can be separated from any suspension or dispersion just by applying an external magnetic field [39]. In the last decade, magnetic nanocomposites such as $CoFe_2O_4/TiO_2$ [12], $CoFe_2O_4/MoS_2$ [40], $CoFe_2O_4/SiO_2/TiO_2$ [41], $CoFe_2O_4$/ZnO [38], Ag/β-Ag_2WO_4/$CoFe_2O_4$ [42] and $CoFe_2O_4$/g-C_3N_4 [43] have been used in the photodegradation of dye molecules from aqueous solution. Recently, the magnetic $MnFe_2O_4/SnO_2$ yolk/shell nanoparticles were synthesized through spray pyrolysis process [44]. The photocatalytic activity of $MnFe_2O_4/SnO_2$ particles was investigated through MO degradation reaction under UV light irritation and the result confirmed the high performance in the photocatalytic activity and stability of the prepared nanoparticles. In another study, magnetic a-Fe_2O_3/SnO_2 composite nanoparticles were synthesized by hydrothermal route [45]. The as-prepared magnetic composites exhibited higher visible light or UV photocatalytic activities compared with bare a-Fe_2O_3 or commercial SnO_2 nanoparticles. Furthermore, magnetically separable Fe_3O_4/SnO_2 nanocomposite was also prepared by hydrothermal and sonochemical methods for the degradation of phenol and rhodamine B under visible light irradiation [46]. The magnetic nanocomposite was developed by incorporating $SnFe_2O_4$ with SnO_2/PANI for the degradation of a mixture containing two dyes namely methylene blue and methyl orange in aqueous solution [47]. However, to the best of authors' knowledge, the development of magnetic $CoFe_2O_4$/SnO_2 nanocomposite and its application in the photocatalytic degradation of organic molecules from aqueous solution have not been reported yet. In order to incorporate magnetic property, SnO_2 can be coupled with $CoFe_2O_4$ nanoparticles.

In the present study, we report the simple wet chemical method for the preparation of magnetically recoverable $CoFe_2O_4/SnO_2$ nanocomposite. The photocatalytic activity of $CoFe_2O_4/SnO_2$ nanoparticles is explored by measuring the degradation of Methylene blue (as a test substance) under UV light irradiation.

2. Experimental setup

2.1. Materials

Anhydrous tin(IV) tetrachloride ($SnCl_4$), 25 wt.% aqueous ammonia, cobalt nitrate hexahydrate ($Co(NO_3)_2{\cdot}6H_2O$) and

ferric nitrate nonahydrate ($Fe(NO_3)_3{\cdot}9H_2O$) were collected from Merck, India. Methylene Blue (MB; $C_{16}H_{18}ClN_3S$) was purchased from Loba Chemie, India. All chemicals were used as received without further purification. The pH of the solution was adjusted to the desired value by dilute HCl and NaOH solutions.

2.2. Synthesis of nanoparticles

2.2.1. Synthesis of tin oxide (SnO_2) nanoparticles

SnO_2 nanoparticles were prepared by precipitation method [48] using anhydrous $SnCl_4$ as precursor and ammonia solution as the precipitating agent. In a typical procedure, 10 mL anhydrous $SnCl_4$ was dissolved in 90 mL deionized water and magnetically stirred for 15 min. Aqueous ammonia (25%) was then added dropwise into the $SnCl_4$ solution under magnetic stirring. A white precipitate was obtained with the addition of ammonia solution. The stirring of the resulting suspension was continued overnight. Subsequently, the precipitate of $Sn(OH)_2$ was separated by centrifugation at 5,800 rpm (for phase separation) and was washed with distilled water until no traces of chloride ion was found in the filtrate. The obtained wet powder was dried in an oven at 110°C overnight followed by calcination in a muffle furnace at 400°C for 2 h. The calcined SnO_2 powder was then ground with agate mortar–pestle and used for further experiment.

2.2.2. Synthesis of $CoFe_2O_4$ nanoparticles

$CoFe_2O_4$ nanoparticles were prepared by co-precipitation method [11] using cobalt nitrate ($Co(NO_3)_2{\cdot}6H_2O$) and iron nitrate ($Fe(NO_3)_3{\cdot}9H_2O$) as the precursors. At first, cobalt nitrate and iron nitrate were prepared separately by dissolving stoichiometric amount of ($Co(NO_3)_2{\cdot}6H_2O$) and ($Fe(NO_3)_3{\cdot}9H_2O$) in 20 mL deionized water. The two solutions were then mixed together and vigorously stirred for 20 min. A dark brown precipitate was obtained after dropwise addition of ammonia solution into the mixed precursor solution. The precipitate was centrifuged (for phase separation) and washed several times until neutral pH was reached. The wet precipitate was then dried at 110°C in an oven overnight followed by calcination in a muffle furnace at 400°C for 5 h. The calcined $CoFe_2O_4$ powder was finely ground with a mortar–pestle to be used for further experiment.

2.2.3. Preparation of SnO_2/$CoFe_2O_4$ nanocomposite

The $CoFe_2O_4/SnO_2$ nanocomposite was synthesized by solid-state reaction method. In a typical procedure, 0.05 g of $CoFe_2O_4$ and 0.95 g of SnO_2 were thoroughly mixed and ground for 1 h through the mortar and pestle. The ground powder was kept in an alumina crucible and calcined at 400°C for 2 h in a furnace. The calcination enhanced the chemical binding among the particles and strengthened the mechanical properties of the nanocomposite. The obtained nanocomposite was then reground to further enhance chemical homogeneity. The resulting powder was then labeled as 5% $CoFe_2O_4/SnO_2$ and used for further experiment. The $CoFe_2O_4/SnO_2$ nanocomposite containing other different percentage of $CoFe_2O_4$ was synthesized in a similar way.

2.3. Characterization

To determine the phase structures and crystallite size of the heterostructure the $CoFe_2O_4/SnO_2$ nanocatalyst powder, X-ray diffraction (XRD) measurement was carried out by X-ray diffractometer (model 3040XPert PRO, Philips, Netherland) using Cu Kα radiation. A continuous scan mode was used to collect 2θ data from 10° to 70°. The average crystallite size of the powder was determined from the diffraction peak widths using Scherrer's formula. The Fourier transform infrared spectroscopy (FT-IR) spectra were obtained with a FT-IR spectrometer (IRPrestige-21, Shimadzu, Japan) using KBr pellet. The surface morphology and corresponding elemental analysis of 5% $CoFe_2O_4/SnO_2$ nanocomposite were inspected by the implementation of field emission scanning electron microscopy (FESEM; JSM-7600F, JEOL, Japan) equipped with EDS. UV-vis diffuse reflectance spectra were recorded at room temperature in the 190–800 nm wavelength range using a UV-vis-NIR spectrometer LAMBDA 750 (PerkinElmer, Inc., USA). Sintered PTFE was used as standard reference. N_2-absorption/desorption isotherm was recorded with an accelerated surface area and porosimetry system ASAP 2020 Plus (Micromeritics Instrument Corporation, USA) instrument at liquid N_2 temperature (77 K). Prior to nitrogen adsorption, sample was degassed at 120°C (10 h) under ultra high vacuum. The specific surface area (S_{BET}) was determined through the Brunauer–Emmett–Teller (BET) equation and pore size distribution was calculated from adsorption branch data by using the Barrett, Joyner, Halenda (BJH) method.

The point of zero charge (pH_{pzc} value) of 5% $CoFe_2O_4/SnO_2$ nanocomposite was estimated following the pH drift method [49,50]. Five samples of 200 mL 0.1 M KNO_3 solution as a background electrolyte were prepared. Then, the initial pH of the electrolyte solution was adjusted to a value between 4 and 8 using 0.1 M HCl or 0.1 M NaOH. 100 mg of 5% $CoFe_2O_4/SnO_2$ nanoparticles was added into 200 mL of the pH-adjusted solution and shaken for 24 h before the final pH (pH_{final}) was observed. The change of solution pH, ΔpH (= $pH_{initial} - pH_{final}$) was plotted against the initial pH, and the pH corresponding to the ΔpH value of zero was taken as the pH_{pzc} of the nanocomposite surface.

2.4. Photocatalytic experiment

The photocatalytic activities of the as-synthesized 5% $CoFe_2O_4/SnO_2$, 3% $CoFe_2O_4/SnO_2$, SnO_2 nanocomposites as well as commercial TiO_2 (Degussa, P-25) were evaluated by the photodegradation of MB in aqueous solution under UV irradiation using 125 W high-pressure mercury lamp (Model: MBFU 125 W E27, Osram Lighting Co., Ltd., China). Photocatalytic experiments were conducted in a reactor system consisting of a UV lamp placed horizontally over a 500 mL Pyrex glass beaker. Cooling water circulation was maintained outside the glass beaker to keep the temperature inside the beaker at 25°C. In each experimental run, 0.1 g of photocatalyst was added to 100 mL of MB dye solution and the resulting suspension was stirred under dark for 30 min to establish adsorption–desorption equilibrium prior to irradiation. The degradation process of MB was assessed by sampling 4 mL solution at appropriate

irradiation time intervals. The concentrations of MB of upper clear liquid after centrifugation were obtained using a UV-vis spectrophotometer (UV-1650, Shimadzu, Japan) by monitoring the absorbance at 664 nm. A blank experiment without UV irradiation but with 5% $CoFe_2O_4/SnO_2$ photocatalysts was performed. The degradation efficiency was defined by the ratio C/C_0, where C_0 is the initial concentration of MB at $t = 0$ and C is the concentration at degradation time t. A blank experiment without UV irradiation but with 5% $CoFe_2O_4/SnO_2$ photocatalysts was performed. The degradation efficiency was defined by the ratio C/C_0, where C_0 is the initial concentration of MB at $t = 0$ and C is the concentration at degradation time t. Chemical oxygen demand (COD) of dye solution was measured using a COD analyzer (Lovibond MD 600 photometer, Tintometer GmbH, Germany).

3. Results and discussion

3.1. Characterization of as-synthesized photocatalysts

The crystalline phases of the as-synthesized photocatalysts were investigated using XRD analysis. The XRD patterns of pure SnO_2 and heterostructure $CoFe_2O_4/SnO_2$ nanoparticles containing 5 wt.% of $CoFe_2O_4$ are shown in Fig. 1a. All the diffraction peaks can readily be indexed to tetragonal rutile (Cassiterite) phase of SnO_2 (JCPDS 41-1445). The interplanar spacing and lattice parameter values obtained for both samples are in good agreement with the standard data. Peaks corresponding to $CoFe_2O_4$ were not seen clearly. In order to identify the crystalline phase of $CoFe_2O_4$ and the presence of other phases of $CoFe_2O_4$, the XRD patterns of all the samples were plotted with enhanced intensity in the region 2θ from 30° to 45° as shown in Fig. 1b. A small peak (Fig. 1B(b)) appeared at 2θ = 35.2° could be ascribed to (311) plane of $CoFe_2O_4$ (JCPDS # 22-1086). The crystallite sizes of SnO_2 estimated from the line broadening of (101) diffraction peak using Scherrer formula were about 5.68 and 8.84 nm in pure SnO_2 nanoparticle and 5% $CoFe_2O_4/SnO_2$ nanocomposite, respectively. The crystallite size of SnO_2 was larger in 5% $CoFe_2O_4/SnO_2$ nanocomposite because pure SnO_2 was further calcined during the preparation of the nanocomposite.

FT-IR spectra of the as-synthesized $CoFe_2O_4$, SnO_2 and $CoFe_2O_4/SnO_2$ samples are shown in Fig. 2. For pure $CoFe_2O_4$ sample (Fig. 2a), the two peaks in the range of 400–700 cm^{-1} may be attributed to the Fe(III)–O and Co(II)–O bond of spinel-type oxide [51,52]. In the FT-IR spectra of heterostructure $CoFe_2O_4/SnO_2$ nanocomposite (Fig. 2b) and pure SnO_2 nanoparticles (Fig. 2c), the peaks at about 3,300–3,420 cm^{-1} and 1,620 cm^{-1}, 640 cm^{-1} can be assigned to the stretching vibration of O–H groups, the bending vibration of adsorbed molecular water and the stretching modes of Sn–O, respectively [36].

The broad absorption band between 400 and 800 cm^{-1} in Fig. 2b may be due to Fe(III)–O and Co(II)–O bond besides Sn–O.

The surface morphology of the as-synthesized 5% $CoFe_2O_4/SnO_2$ composite nanoparticles was studied using scanning electron microscope (SEM) as shown in Fig. 3a. The figure exhibits that the nanoparticles are spherical in shape with an average size of about 24 nm. The selected area of SEM image of Fig. 3a was two times enlarged that confirmed the spherical shape of the as-prepared nanoparticles. The larger particles observed in the figure may be aggregates of the smaller particles.

The composition and the presence of $CoFe_2O_4$ in the as-synthesized samples were confirmed by energy dispersive X-ray analysis and the results are shown in Fig. 4. All of the peaks in the figure were ascribed to Co, Fe, Sn and O, and no peaks of other elements were observed. Therefore, it can be concluded that the as-synthesized samples were composed of only Co, Fe, Sn and O, which was in good agreement with the above XRD results. The absence of other elements in the sample implies the high purity of the as-synthesized samples. Elemental analysis also confirmed 5.14 wt.% $CoFe_2O_4$ content in $CoFe_2O_4/SnO_2$, which

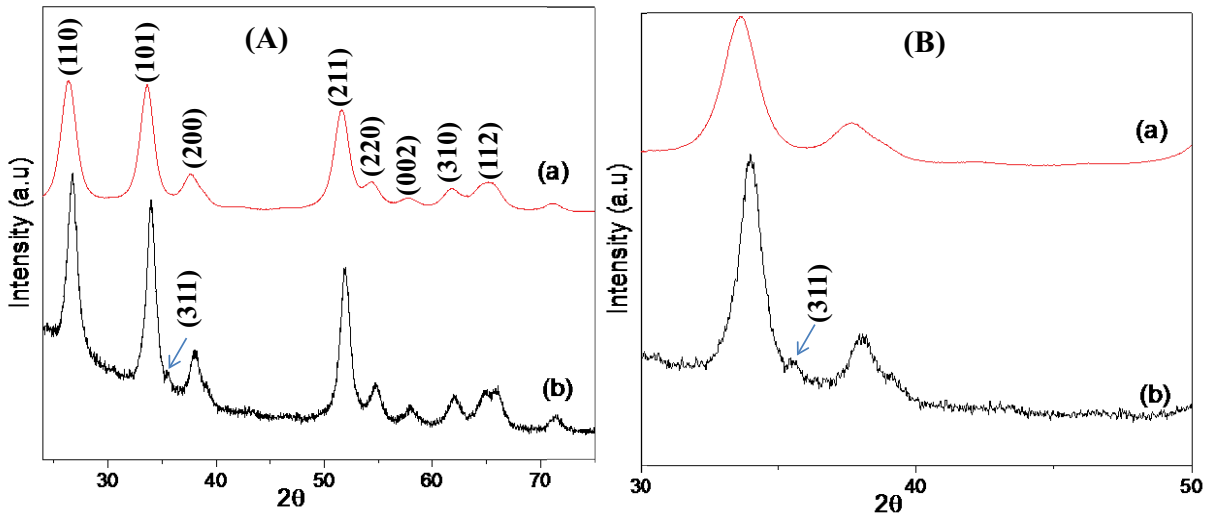

Fig. 1. XRD pattern of SnO_2 and 5% $CoFe_2O_4/SnO_2$ in the 2θ region of (A) 25°–75° and (B) 30°–50°. (a) SnO_2 (red line) and (b) 5% $CoFe_2O_4/SnO_2$ (black line).

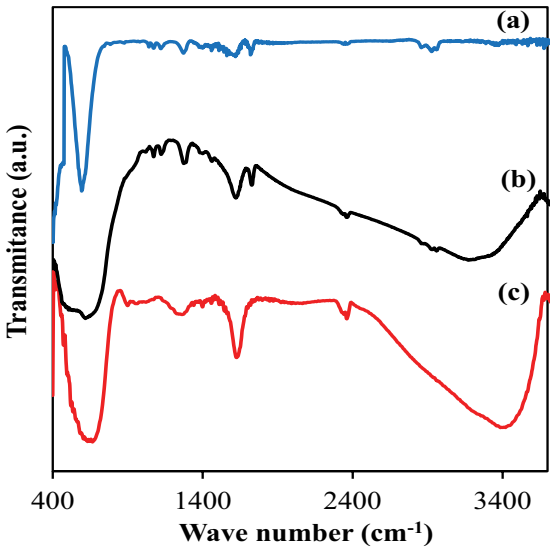

Fig. 2. FT-IR spectra of (a) $CoFe_2O_4$ (blue line), (b) 5% $CoFe_2O_4/SnO_2$ (black line) and (c) SnO_2 (red line).

was very close to the theoretical mass of $CoFe_2O_4$ content in 5 wt.% $CoFe_2O_4/SnO_2$ nanocomposite.

The optical property such as band gap of as-synthesized nanoparticles was calculated by means of the optic absorption spectrum. When a semiconductor absorbs photons of energy larger than the band gap of the semiconductor, an electron is transferred from the valence band to the conduction band where there occurs an abrupt increase in the absorbency of the material to the wavelength corresponding to the band gap energy. The optical properties of the various samples prepared were investigated by UV-Visible diffuse reflectance (UV-Vis DR). The UV-Vis DR spectra of the as-synthesized samples are shown in Fig. 5a. The pure SnO_2 and 5% $CoFe_2O_4/SnO_2$ nanocomposite exhibited the characteristic spectrum of SnO_2 with its fundamental sharp edge around 342 nm. The composite showed an extra absorption peak in the visible region, which was contributed by $CoFe_2O_4$. Based on their absorption spectra, the band gap energy (E_g) of direct band gap semiconductor such as SnO_2 nanoparticles was calculated from the following equation, $\alpha(h\nu) = A(h\nu - E_g)^{1/2}$, where α,

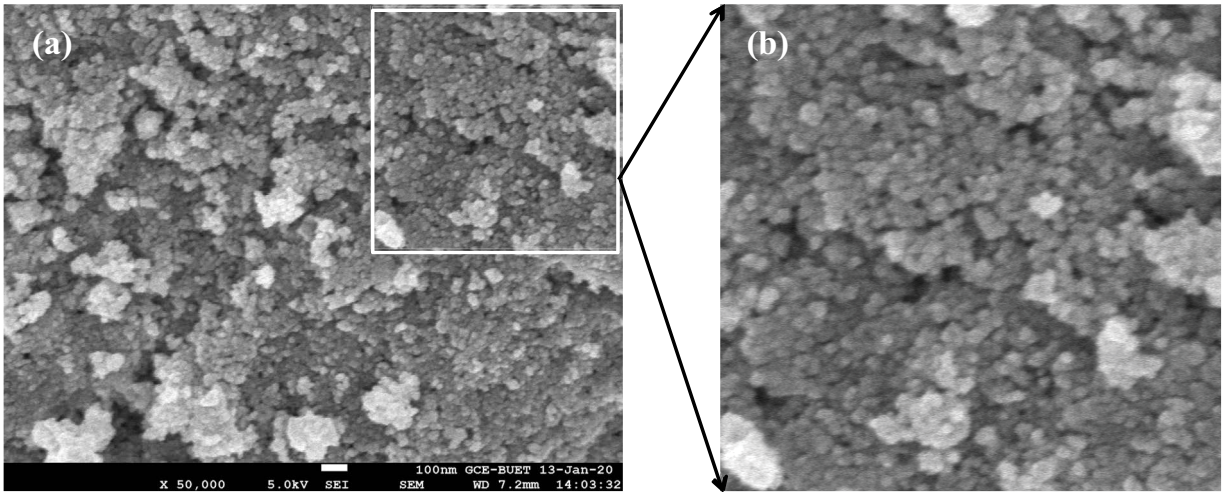

Fig. 3. (a) SEM image of 5% $CoFe_2O_4/SnO_2$ composite nanoparticles and (b) two times enlarged SEM image of selected area.

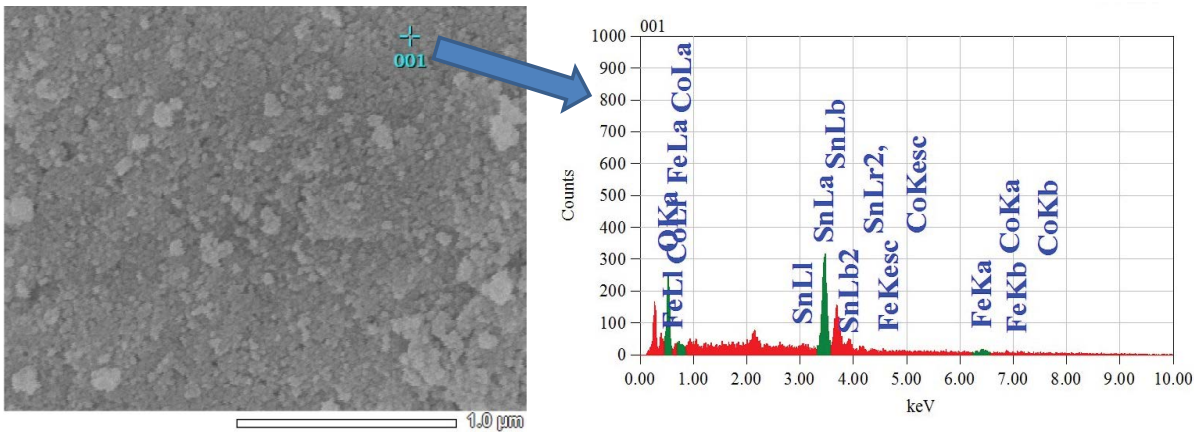

Fig. 4. Energy-dispersive X-ray spectrum of 5% $CoFe_2O_4/SnO_2$ nanoparticles.

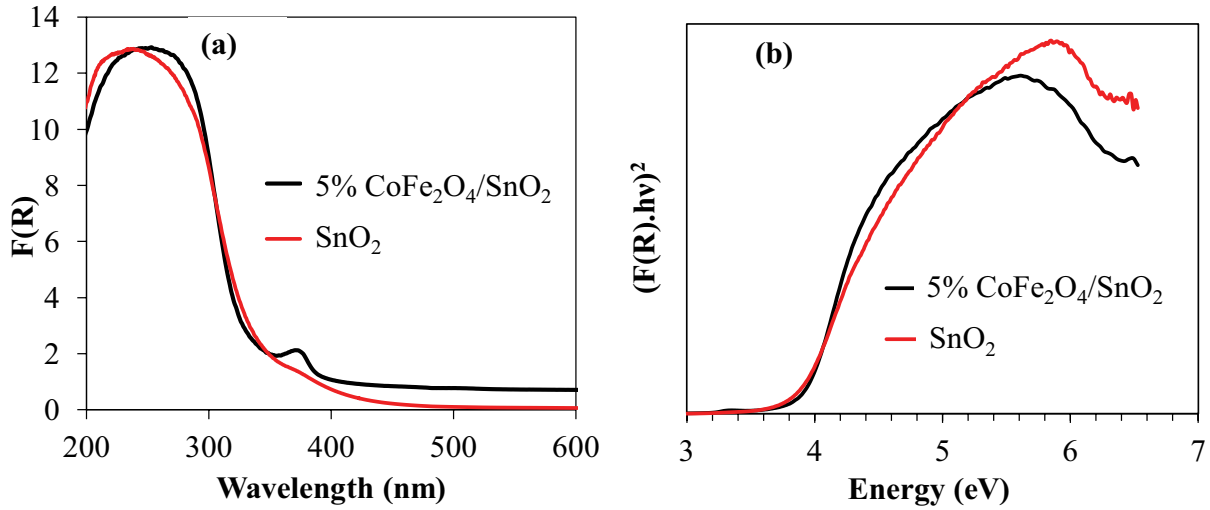

Fig. 5. UV-visible diffuse reflectance spectra (a) and plots of $(F(R)h\nu)^2$ vs. photon energy ($h\nu$) (b) of as-synthesized SnO_2 (red) and 5% $CoFe_2O_4/SnO_2$ (black) nanoparticles.

ν, E_g and A are the absorption coefficient, light frequency, band gap energy and a constant, respectively [53]. The energy band gap was calculated by extrapolating a straight line to the abscissa axis, where α is zero, for $E_g = h\nu$ [54]. It is generally admitted that the absorption coefficient (α) can be replaced by the remission function $F(R)$. The later can be written in terms of diffused reflectance (R) according to the Kubelka-Munk theory: $\alpha/s = F(R) = (1 - R)^2/(2R)$, where s is scattering coefficient [55]. The band gap energies (E_g values) of the as-synthesized samples can thus be estimated from a plot of $(F(R)h\nu)^2 = f(h\nu)$, the intercepts of the tangents yielding the band gap energies of the as-synthesized samples. The calculated band gap energy for 5% $CoFe_2O_4/SnO_2$ was found to be 3.7 eV from the extrapolation of the corresponding plot (Fig. 5b), which was comparable with that of pure SnO_2. The calculated band gap energies for SnO_2 and $CoFe_2O_4$ were 3.7 and 2.5 eV, respectively and were in good agreement with the literature [34,56].

The N_2 adsorption–desorption isotherms and the corresponding BJH pore size distribution curve for 5% $CoFe_2O_4/SnO_2$ sample are shown in Figs. 6a and b, respectively. Based on IUPAC classification, Fig. 6a exhibits type IV isotherm with a H2 type hysteresis loop at relative pressure (P/P_0) higher than 0.4, that demonstrated the presence of mesopores in as-synthesized photocatalyst [57,58]. The observed H2 type hysteresis loop is a characteristic of solids consisting of particles crossed by nearly cylindrical channels (nonuniform size or shape) or made by aggregates (consolidated) or agglomerates (unconsolidated) of spheroidal particles [59]. The BET surface area and pore volume of 5% $CoFe_2O_4/SnO_2$ sample were found to be 40.73 m^2/g and 0.11 cm^3/g, respectively. The mesoporous structure of the sample was confirmed by analysis of pore size distribution presented in Fig. 6b. Fig. 6b evidenced that the pore size distribution of 5% $CoFe_2O_4/SnO_2$ nanocomposites (BJH model applied to the adsorption branch of the sorption isotherm) was rather large ranging from 3 to 30 nm (mesopore range: 2–50 nm) with an adsorption average pore diameter of 10.12 nm.

Taking into account the magnetic separation applications of $CoFe_2O_4/SnO_2$ nanoparticles as photocatalyst, magnetic response of the nanoparticles in an externally applied magnetic field created with a neodymium magnet was checked. Fig. 7 shows the photograph of 5% $CoFe_2O_4/SnO_2$ nanoparticles separation from its suspension by an external magnet field. As shown in Fig. 7, in the presence of externally applied magnetic field, the magnetic $CoFe_2O_4/SnO_2$ nanoparticles gathered quickly without residues left in the solution. This property of magnetic attraction of as-prepared nanoparticles is quite appropriate for their separation after use in photocatalytic process. The magnetic property is due to the presence of $CoFe_2O_4$ in the nanocomposites. Therefore, it can be concluded that the magnetic response of the as-prepared nanoparticles will prevent the loss of materials and high cost which will lead to the industrial applications of the nanoparticles for environment remediation.

As shown in Fig. 8, the pH corresponding to the ΔpH value of zero (i.e., $pH_{final} = pH_{initial}$) is at 4.5, that is, the pH at the point of zero charge (pH_{pzc}) of 5% $CoFe_2O_4/SnO_2$ nanoparticles is about pH 4.5. The surface of nanoparticles becomes positively and negatively charged at pH below and above pH_{pzc}, respectively.

3.2. Photocatalytic studies

The photocatalytic activity of the as-synthesized $CoFe_2O_4/SnO_2$ nanocomposites has been evaluated by testing the degradation of methylene blue under UV light irradiation. As depicted in Fig. 9a, the color of the solution changed gradually with time suggesting that the chromophoric structure of MB was decomposed. Furthermore, blank experiment with photocatalyst in the absence of irradiation was carried out to rationalize the photocatalytic activity of the as-synthesized $CoFe_2O_4/SnO_2$ photocatalyst. The blank test result showed that the change in concentration of MB was insignificant suggesting that the MB could not be neither decomposed nor adsorbed with only photocatalyst and in absence of UV irradiation (Fig. 9b).

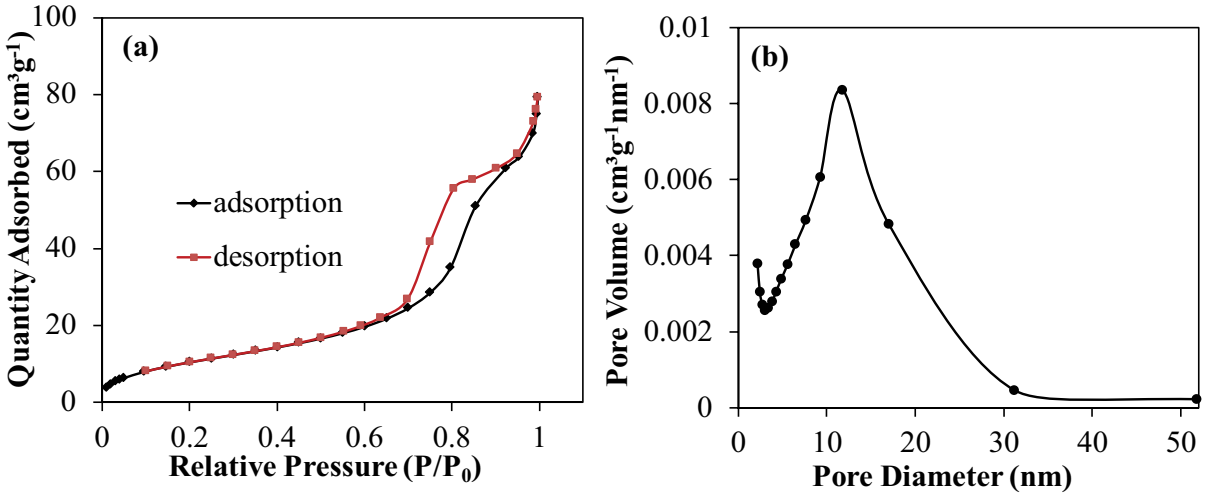

Fig. 6. Nitrogen adsorption–desorption isotherms (a) and pore size distribution curve (b) of 5% $CoFe_2O_4/SnO_2$ photocatalyst.

Fig. 7. Photographs of the magnetic separation of magnetic 5% $CoFe_2O_4/SnO_2$ nanoparticles by an external magnetic field.

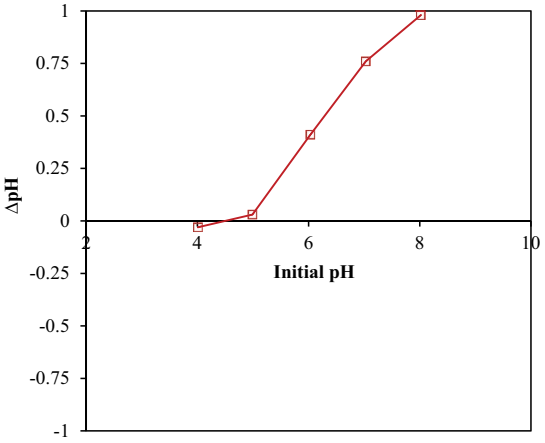

Fig. 8. Determination of pH_{pzc} of 5% $CoFe_2O_4/SnO_2$ nanocomposite by the pH drift method.

In order to compare the photocatalytic activity of 5% $CoFe_2O_4/SnO_2$, 3% $CoFe_2O_4/SnO_2$, SnO_2 and commercial TiO_2 (Degussa, P-25, Germany), the photocatalytic degradation of MB under UV illumination was investigated and the obtained results were illustrated in Fig. 9b. From Fig. 9b, it is observed that the 5% $CoFe_2O_4/SnO_2$ nanocatalyst showed higher photocatalytic degradation efficiency compared with P-25 and SnO_2. After 50 min of photocatalytic reaction, the $CoFe_2O_4/SnO_2$ catalyst exhibited almost total dye degradation, meanwhile the SnO_2 and P-25 catalysts showed 95.0% and 87.0% of dye degradations, respectively. As $CoFe_2O_4/SnO_2$ nanocatalyst containing 5 wt.% $CoFe_2O_4$ showed higher photocatalytic activity, 5% $CoFe_2O_4/SnO_2$ nanocomposites will be used in the subsequent experiment in order to investigate the effect of various parameters on the photocatalytic degradation efficiency.

In photocatalysis system, the solution pH is an important parameter because it affects not only the surface charge

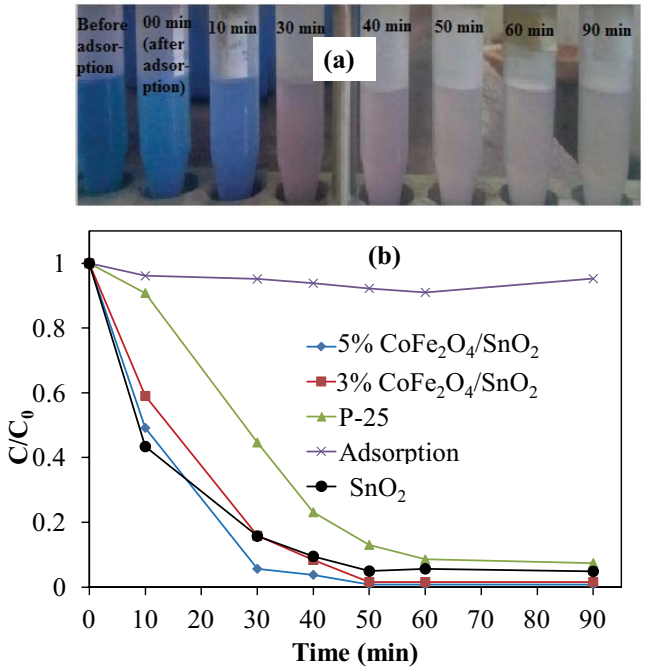

Fig. 9. (a) Color change of MB solution with time under UV light irradiation in the presence of 5% $CoFe_2O_4/SnO_2$; (b) photocatalytic activity of 5% $CoFe_2O_4/SnO_2$, 3% $CoFe_2O_4/SnO_2$, SnO_2 and P-25 under UV irradiation (experimental conditions: initial dye solution concentration = 10 mg/L; volume = 100 mL, pH = 9; catalyst dose = 1 g/L; irradiation time = 90 min).

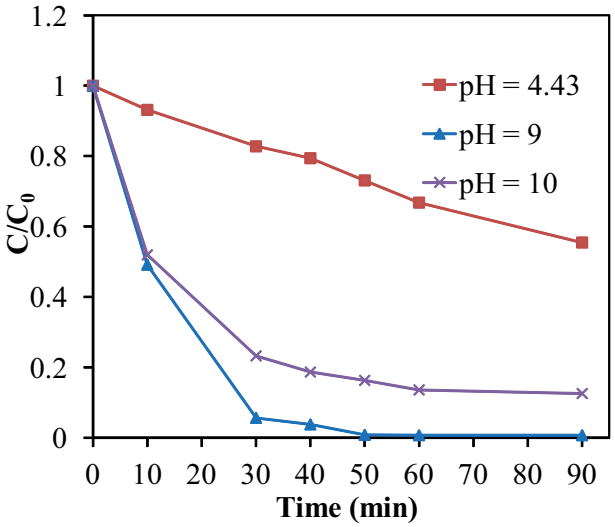

Fig. 10. Effect of pH on the photocatalytic degradation of MB onto 5% $CoFe_2O_4/SnO_2$ nanoparticles (experimental conditions: initial dye solution concentration = 10 mg/L; volume = 100 mL, pH = 4.43, 9 and 10; catalyst dose = 1 g/L; irradiation time = 90 min).

on the metal oxide catalyst but also the formation of hydroxyl radicals by the reaction between hydroxide ions and photo-generated holes on the catalyst surface [60–62]. The effect of solution pH on the photocatalytic degradation of MB was studied at the initial pH 4.43, 9 and 10. Fig. 10 shows the pH effect on the photodegradation efficiency of MB. As shown in Fig. 9, the rate of MB decomposition over 5% $CoFe_2O_4/SnO_2$ catalyst is clearly influenced by dye solution pH and the catalyst is more effective in alkaline environment. Considering the positive charge of cationic MB dye in solution, the effect of pH on the photocatalytic degradation of MB can be rationalized on the basis of electrostatic adsorption model where cations are more readily accumulated at the negative sites on the $CoFe_2O_4/SnO_2$ nanocomposites. This can be explained on the basis of the point of zero charge (pH_{pzc}) of $CoFe_2O_4/SnO_2$ particle. As the point of zero charge of $CoFe_2O_4/SnO_2$ nanoparticles is 4.5, the surface of the catalyst gets positively charge when the solution pH is lower than 4.5. As a result, the cationic dye MB is poorly adsorbed at lower pH due to electrostatic repulsion between dye cations and positively charged catalyst surface, which leads to the reduction of photocatalytic degradation. In contrast, enhanced degradation efficiency is observed at alkaline pH range. This can be explained by the facts that the formation of active •OH radicals is favored at higher pH due to the presence of more available hydroxyl ions on the catalyst surface and consequent improvement in the transfer of holes to the adsorbed hydroxyls [63]. In addition, the adsorption of MB, a cationic dye, is better on the negatively charged catalyst surface due to electrostatic attraction under pH > pH_{pzc} (zero point charge) conditions result in enhanced photodegradation efficiency.

The influence of photocatalyst dose on the photocatalytic degradation of MB was studied by employing different doses of 5% $CoFe_2O_4/SnO_2$ nanoparticles varying from 0.5 to 1 g/L and the result is presented in Fig. 11a. As shown in Fig. 11a, the degradation of MB was significantly influenced by the dose of catalyst. The percentage degradation of MB was found to increase from 79% to 99% with the increase in catalyst dose from 0.5 to 1 g/L. This is because of the increased catalyst surface area, improved photon absorption and greater number of active centers for the photocatalytic reaction at higher dose of the photocatalyst. Moreover, the adsorption of dye on the catalyst increases with the increase in catalyst dose resulting in an enhanced degradation of MB [64].

The initial concentration of organic dyes strongly affects the photodegradation reaction. The photocatalytic degradation behavior of MB onto 5% $CoFe_2O_4/SnO_2$ nanoparticles was studied by varying the initial dye solution concentrations from 10 to 20 mg/L at constant catalyst loading (1 g/L, pH 9) and the results are shown in Fig. 11b. As expected, the degradation rate decreases with the increase in dye solution concentration. This is due to the fact that the adsorption of dye onto the catalyst surface active sites increases with the increase in dye solution concentration. Therefore, the potential active sites for the adsorption of OH^- ion decrease causing a lower generation rate of •OH radical, which is the primary oxidant required for a high degradation performance. Again, with the increase in dye solution concentration, the amount of photon absorbed by the dye molecules increases, resulting in a lower absorption of photon by the catalyst particles. Consequently, the photoexcitation rate of the catalyst decreases, which leads to a lower photodegradation rate.

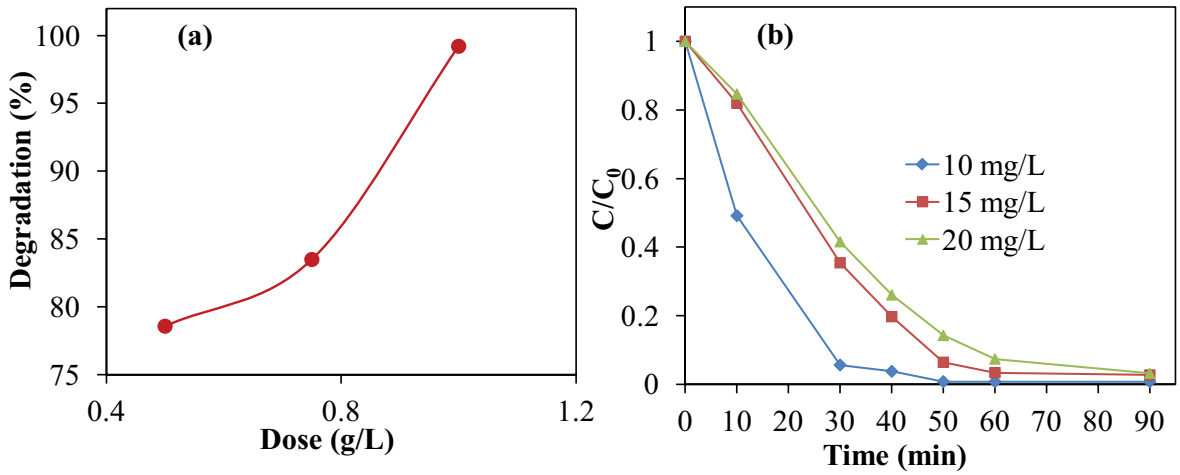

Fig. 11. (a) Effect of catalyst (5% $CoFe_2O_4/SnO_2$ nanoparticles) concentration on the photodegradation of MB (experimental conditions: initial dye solution concentration = 10 mg/L; volume = 100 mL; pH = 9; catalyst dose = 0.5–1 g/L; irradiation time = 90 min) and (b) effect of initial dye solution concentration on the photocatalytic degradation of MB onto 5% $CoFe_2O_4/SnO_2$ nanoparticles (experimental conditions: initial dye solution concentration = 10–20 mg/L; volume = 100 mL; pH = 9; catalyst dose = 1 g/L; irradiation time = 90 min).

Among the initial dye solution concentrations studied, the 10 mg/L concentration offered the highest rate for MB degradation. Therefore, 10 mg/L was fixed as optimized MB concentration for all the experiments.

To investigate the reusability and stability of the photocatalyst, recycling tests were conducted. Fig. 12 shows the repetitive photodegradation of MB onto the 5 wt.% $CoFe_2O_4/SnO_2$ catalyst in three consecutive cycles. As shown in Fig. 12, there was no significant change in photocatalytic activity of the catalyst in three successive runs which indicated the stability and reusability of the photocatalyst for the degradation of MB. After 90 min of photocatalytic reaction under UV-light irradiation, the photodegradation efficiencies of 5 wt.% $CoFe_2O_4/SnO_2$ nanocomposite in three successive cycles were 99.21%, 97.77% and 96.13%, respectively.

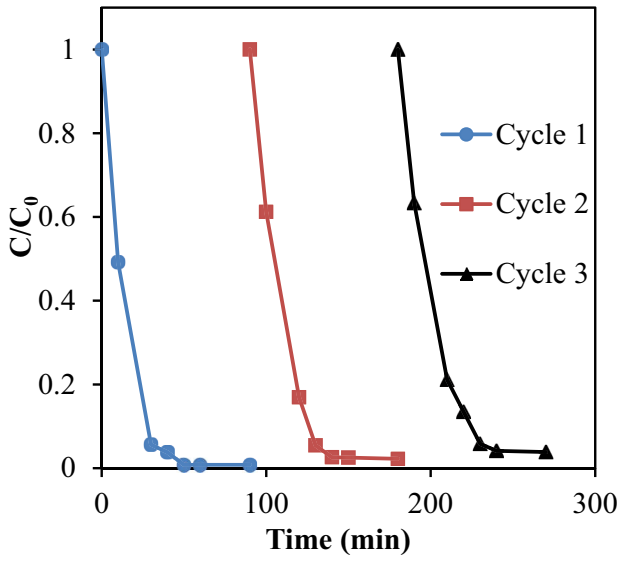

Fig. 12. Recyclability of the 5 wt.% $CoFe_2O_4/SnO_2$ photocatalyst in the photodegradation of MB under UV-light irradiation.

4. COD analysis

COD of MB solutions before and after photocatalytic degradation was measured (using Lovibond MD 600 photometer) in order to investigate the mineralization status of the photodegraded solution. The COD value of MB solution (C_0 = 10 mg/L) before photodegradation under UV irradiation was about 23 mg/L. In contrast, no COD value of the same sample was observed after 90 min of photodegradation under UV irradiation in the presence of 5% $CoFe_2O_4/SnO_2$ catalyst, which indicated that the MB was completely mineralized to CO_2 and H_2O by the photocatalytic degradation.

5. Photocatalytic mechanism

In order to reveal the band alignment of $CoFe_2O_4/SnO_2$ heterostructure, the positions of the conduction band (CB) and valence band (VB) edges of $CoFe_2O_4$ and SnO_2 were calculated by the following Mulliken electronegativity equation [65]:

$$E_{CB} = \chi - E_e - 0.5E_g \quad (1)$$

$$E_{VB} = \chi - E_e + 0.5E_g \quad (2)$$

where χ, E_{VB}, E_{CB} and E_g represent the absolute electronegativity, the valance band edge potential, conduction band edge potential and the band gap energy of the semiconductor, respectively. E_e is the energy of free electrons on the hydrogen scale (about 4.5 eV vs. NHE). The values of

χ are 5.47 and 6.25 eV for $CoFe_2O_4$ and SnO_2, respectively [51,65]. The calculated values of E_{CB} and E_{VB} for $CoFe_2O_4$ are –0.28 and 2.22 eV, and for SnO_2 are –0.1 and 3.6 eV, respectively. Based on the above calculation, the mechanism for the photocatalytic degradation of MB by $CoFe_2O_4/SnO_2$ nanocatalyst was proposed in Fig. 13. As shown in Fig. 13, the conduction band edge potential and valence band edge potential for $CoFe_2O_4$ were, respectively, more negative and less positive than those for SnO_2. Under illumination with UV light, both $CoFe_2O_4$ and SnO_2 were activated, and electrons (e) in the VB of both the semiconductor oxides were excited to the CB, with the same amount of holes (h) left in VB. Due to the difference of band edge position, the excited-state electrons at the conduction band (CB) of $CoFe_2O_4$ can easily migrate to the CB of SnO_2. Meanwhile, the photoinduced holes at the valence band (VB) of SnO_2 can readily be injected into the VB of $CoFe_2O_4$. Therefore, photogenerated electrons and holes migrated to the opposite directions, which effectively improved the charge separation efficiency and reduced the recombination probability of photoinduced charge carriers. Consequently, the photocatalytic efficiency of $CoFe_2O_4/SnO_2$ nanocomposite was improved. The accumulated electrons in the CB of SnO_2 can be captured by the adsorbed O_2 to generate superoxide anion radicals ($O_2^{\bullet-}$). The super oxide radicals then reacted with water (H_2O) to produce hydroxyl radicals ($OH^{\bullet}$). The holes in the VB of $CoFe_2O_4$ reacted with the absorbed H_2O molecules or hydroxyl groups on the surface of $CoFe_2O_4$ to form the hydroxyl radical species ($OH^{\bullet}$). Finally, the generated active species such as hydroxyl radical mineralized the MB dye molecules to the final degradation products (e.g., CO_2, H_2O).

6. Conclusion

Magnetically separable $CoFe_2O_4/SnO_2$ nanocatalyst was successfully prepared via a simple chemical precipitation technique followed by calcination in air, and used as a novel heterogeneous photocatalyst for the degradation of methylene blue (MB) dye from aqueous solution under UV irradiation. The 5% $CoFe_2O_4/SnO_2$ nanocomposite showed higher photocatalytic activity than pure SnO_2 and commercial TiO_2 (Degussa, P-25, Germany). The 5% $CoFe_2O_4/SnO_2$ could degrade more than 99% of MB (10 mg/L) within 50 min. The photocatalytic performance of 5% $CoFe_2O_4/SnO_2$ was greatly influenced by the initial dye solution pH. The nanoparticles could be easily separated by the application of external magnetic field for reuse. Therefore, the $CoFe_2O_4/SnO_2$ nanocomposite exhibits excellent properties for practical application in the photocatalytic treatment of effluent liquids containing organic pollutants.

Acknowledgments

The authors gratefully acknowledge financial support from Shahjalal University of Science and Technology (SUST) Research Centre (Grant No.: AS/2018/3/35) for conducting this research work. The authors would also like to thank

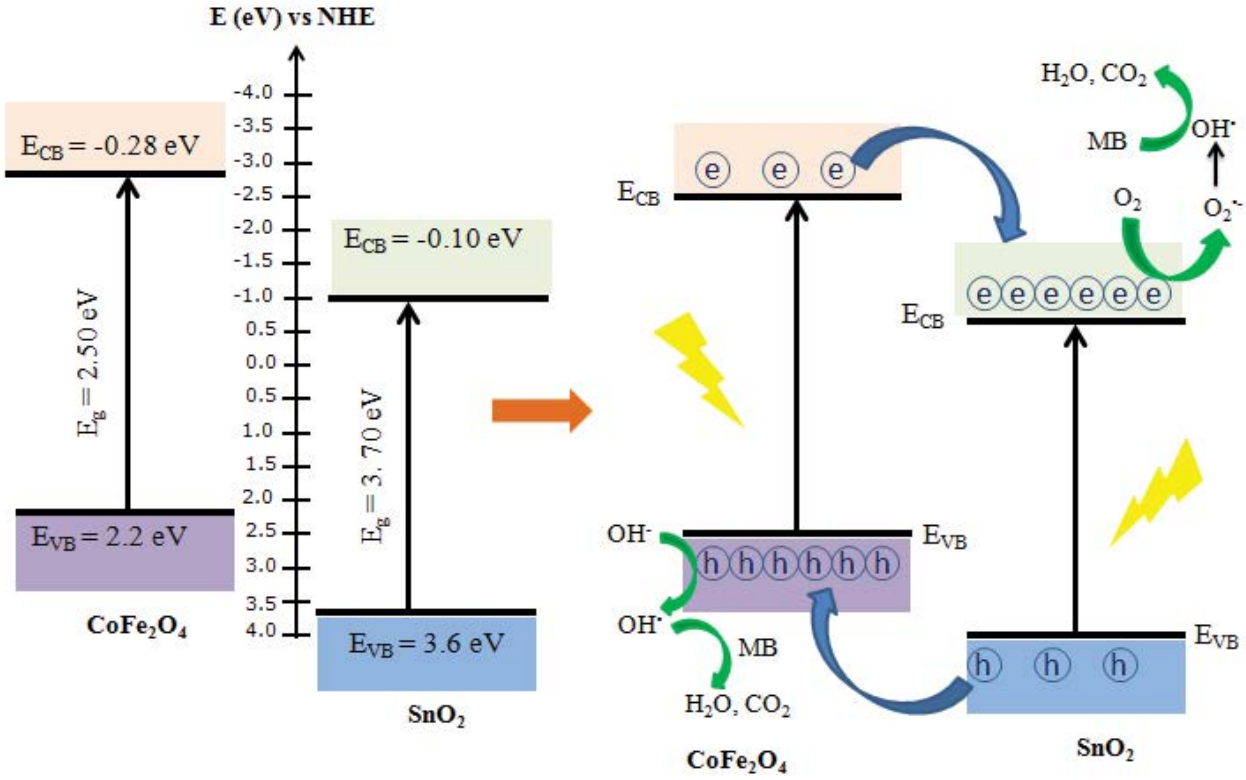

Fig. 13. Band alignment of $CoFe_2O_4/SnO_2$ heterostructure photocatalyst and mechanism for the degradation of MB dye under UV light irradiation.

Center of Excellence, SUST for providing equipment to determine BET surface area and band gap energy.

References

[1] M. Imran, D.E. Crowley, A. Khalid, S. Hussain, M.W. Mumtaz, M. Arshad, Microbial biotechnology for decolorization of textile wastewaters, Rev. Environ. Sci. Bio/Technol., 14 (2015) 73–92.

[2] M.M. Hassan, C.M. Carr, A critical review on recent advancements of the removal of reactive dyes from dye house effluent by ion-exchange adsorbents, Chemosphere, 209 (2018) 201–219.

[3] Z. Noorimotlagh, R.D.C. Soltani, A. Khataee, S. Shahriyar, H. Nourmoradi, Adsorption of a textile dye in aqueous phase using mesoporous activated carbon prepared from Iranian milk vetch, J. Taiwan Inst. Chem. Eng., 45 (2014) 1783–1791.

[4] M.M.R. Khan, M.Z.B. Mukhlish, M.S.I. Mazumder, K. Ferdous, D.M.R. Prasad, Z. Hassan, Uptake of Indosol Dark-blue GL dye from aqueous solution by water hyacinth roots powder: adsorption and desorption study, Int. J. Environ. Sci. Technol., 11 (2014) 1027–1034.

[5] M.Z.B. Mukhlish, Y. Horie, T. Nomiyama, Flexible alumina-silica nanofibrous membrane and its high adaptability in reactive red-120 dye removal from water, Water Air Soil Pollut., 228 (2017) 371.

[6] Y. Fu, L. Qin, D. Huang, G. Zeng, C. Lai, B. Li, J. He, H. Yi, M. Zhang, M. Cheng, X. Wen, Chitosan functionalized activated coke for Au nanoparticles anchoring: green synthesis and catalytic activities in hydrogenation of nitrophenols and azo dyes, Appl. Catal. B, 255 (2019) 117740.

[7] Y. Fu, P. Xu, D. Huang, G. Zeng, C. Lai, L. Qin, B. Li, J. He, H. Yi, M. Cheng, C. Zhang, Au nanoparticles decorated on activated coke via a facile preparation for efficient catalytic reduction of nitrophenols and azo dyes, Appl. Surf. Sci., 473 (2019) 578–588.

[8] S.P. Kim, M.Y. Choi, H.C. Choi, Photocatalytic activity of SnO_2 nanoparticles in methylene blue degradation, Mater. Res. Bull., 74 (2016) 85–89.

[9] H. Zhou, D.W. Smith, Advanced technologies in water and wastewater treatment, J. Environ. Eng. Sci., 1 (2002) 247–264.

[10] M.Z.B. Mukhlish, M.R. Khan, M.S. Islam, M.I. Nazir, J.S. Snigdha, R. Akter, H. Ahmad, Decolorization of reactive dyes from aqueous solution using combined coagulation-flocculation and photochemical oxidation (UV/H_2O_2), Sustain. Chem. Eng., 1 (2020) 51–61. Available at: http://ojs.wiserpub.com/index.php/SCE/article/view/214/143

[11] P. Sathishkumar, R.V. Mangalaraja, S. Anandan, M. Ashokkumar, $CoFe_2O_4/TiO_2$ nanocatalysts for the photocatalytic degradation of Reactive Red 120 in aqueous solutions in the presence and absence of electron acceptors, Chem. Eng. J., 220 (2013) 302–310.

[12] C.-J. Li, J.-N. Wang, B. Wang, J. RuGong, Z. Lin, A novel magnetically separable $TiO_2/CoFe_2O_4$ nanofiber with high photocatalytic activity under UV–vis light, Mater. Res. Bull., 47 (2012) 333–337.

[13] A.B.A. Baig, V. Rathinam, J. Palaninathan, Fabrication of Zr-doped SnO_2 nanoparticles with synergistic influence for improved visible-light photocatalytic action and antibacterial performance, Appl. Water Sci., 10 (2020) 85.

[14] P.V. Viet, C.M. Thi, L.V. Hieu, The high photocatalytic activity of SnO_2 nanoparticles synthesized by hydrothermal Method, J. Nanomater., 2016 (2016) 4231046.

[15] A. Kumar, G. Pandey, Desalination and water treatment photocatalytic degradation of Eriochrome Black-T by the $Ni:TiO_2$ nanocomposites, Desal. Water Treat., 71 (2017) 406–419.

[16] O. Solcova, L. Spacilova, Y. Maleterova, M. Morozova, M. Ezechias, Z. Kresinova, Photocatalytic water treatment on TiO_2 thin layers, Desal. Water Treat., 57 (2016) 11631–11638.

[17] A.M. Al-Hamdi, U. Rinner, M. Sillanpääa, Tin dioxide as a photocatalyst for water treatment: a review, Process Saf. Environ. Prot., 107 (2017) 190–205.

[18] M.N. Chong, B. Jin, C.W.K. Chow, C. Saint, Recent developments in photocatalytic water treatment technology: a review, Water Res., 44 (2010) 2997–3027.

[19] N. Wu, H. Wei, L. Zhang, Efficient removal of heavy metal ions with biopolymer template synthesized mesoporous titania beads of hundreds of micrometers size, Environ. Sci. Technol., 46 (2012) 419–425.

[20] B. Krishnakumar, M. Swaminathan, Solar photocatalytic degradation of Naphthol Blue Black, Desal. Water Treat., 51 (2013) 6572–6579.

[21] M.H.S. Abadi, M.N. Hamidon, A.H. Shaari, N. Abdullah, R. Wagiran, SnO_2/Pt thin film laser ablated gas sensor array, Sensors (Basel), 11 (2011) 7724–7735.

[22] Z. Tebby, M.T. Uddin, Y. Nicolas, C. Olivier, T. Toupance, C. Labrugère, L. Hirsch, Low-temperature UV processing of nanoporous SnO_2 layers for dye-sensitized solar cells, ACS Appl. Mater. Interfaces, 3 (2011) 1485–1491.

[23] Y. Fukai, Y. Kondo, S. Mori, E. Suzuki, Highly efficient dye-sensitized SnO_2 solar cells having sufficient electron diffusion length, Electrochem. Commun., 9 (2007) 1439–1443.

[24] K.L. Chopra, S. Major, D.K. Pandya, Transparent conductors – a status review, Thin Solid Films, 102 (1983) 1–46.

[25] H.-M. Xiong, K.-K. Zhao, X. Zhao, Y.-W. Wang, J.-S. Chen, Elucidating the conductivity enhancement effect of nano-sized SnO_2 fillers in the hybrid polymer electrolyte PEO–SnO_2–$LiClO_4$, Solid State Ionics, 159 (2003) 89–95.

[26] E. Abdelkader, L. Nadjia, V. Rose-Noëlle, Adsorption of Congo red azo dye on nanosized SnO_2 derived from sol–gel method, Int. J. Ind. Chem., 7 (2016) 53–70.

[27] V.K. Vidhu, D. Philip, Phytosynthesis and applications of bioactive SnO_2 nanoparticles, Mater. Charact., 101 (2015) 97–105.

[28] G. Elango, S.M. Roopan, Efficacy of SnO_2 nanoparticles toward photocatalytic degradation of methylene blue dye, J. Photochem. Photobiol. B, 155 (2016) 34–38.

[29] K. Anandan, V. Rajendran, Influence of dopant concentrations (Mn = 1, 2 and 3 mol%) on the structural, magnetic and optical properties and photocatalytic activities of SnO_2 nanoparticles synthesized via the simple precipitation process, Superlattices Microstruct., 85 (2015) 185–197.

[30] K. Kogo, H. Yoneyama, H. Tamura, Photocatalytic oxidation of cyanide on platinized titanium dioxide, J. Phys. Chem., 84 (1980) 1705–1710.

[31] F. Amano, E. Ishinaga, A. Yamakata, Effect of particle size on the photocatalytic activity of WO_3 particles for water oxidation, J. Phys. Chem. C, 117 (2013) 22584–22590.

[32] A.L. Rudd, C.B. Breslin, Photo-induced dissolution of zinc in alkaline solutions, Electrochim. Acta, 45 (2000) 1571–1579.

[33] C.M. Ma, G.B. Hong, S.C. Lee, Facile Synthesis of tin dioxide nanoparticles for photocatalytic degradation of congo red dye in aqueous solution, Catalysts, 10 (2020) 792.

[34] M.T. Uddin, Y. Nicolas, C. Olivier, T. Toupance, L. Servant, M.M. Müller, H.J. Kleebe, J. Ziegler, W. Jaegermann, Nano-structured SnO_2–ZnO heterojunction photocatalysts showing enhanced photocatalytic activity for the degradation of organic dyes, Inorg. Chem., 51 (2012) 7764–7773.

[35] X. Zhu, Z. Guo, P. Zhang, Guo, G. Du, R. Zeng, H. Liu, Z. Chen, Tin oxide thin film with three-dimensional ordered reticular morphology as a lithium ion battery anode, ChemPhys Chem, 10 (2009) 3101–3104.

[36] M.T. Uddin, Y. Sultana, M.A. Islam, Nano-sized SnO_2 photocatalysts: synthesis, characterization and their application for the degradation of methylene blue dye, J. Sci. Res., 8 (2016) 399–411.

[37] X. Zhang, C. Shao, Z. Zhang, J. Li, P. Zhang, M. Zhang, J. Mu, Z. Guo, P. Liang, Y. Liu, In situ generation of well-dispersed ZnO quantum dots on electrospun silica nanotubes with high photocatalytic activity, ACS Appl. Mater. Interfaces, 4 (2012) 785–790.

[38] G. Zhang, W. Xu, Z. Li, W. Hu, Y. Wang, Preparation and characterization of multi-functional $CoFe_2O_4$–ZnO nanocomposites, J. Magn. Magn. Mater., 321 (2009) 1424–1427.

[39] Y.H. Hou, Y.J. Zhao, Z.W. Liu, H.Y. Yu, X.C. Zhong, W.Q. Qiu, D.C. Zeng, L.S. Wen, Structural, electronic and magnetic properties of partially inverse spinel $CoFe_2O_4$: a first-principles study, J. Phys. D, 43 (2010) 445003.

[40] B. Ren, W. Shen, L. Li, S. Wu, W. Wang, 3D $CoFe_2O_4$ nanorod/flower-like MoS_2 nanosheet heterojunctions as recyclable visible light-driven photocatalysts for the degradation of organic dyes, Appl. Surf. Sci., 447 (2018) 711–723.
[41] Z. Yang, Y. Shi, B. Wang, Photocatalytic activity of magnetically anatase TiO_2 with high crystallinity and stability for dyes degradation: insights into the dual roles of SiO_2 interlayer between TiO_2 and $CoFe_2O_4$, Appl. Surf. Sci., 399 (2017) 192–199.
[42] M. Ghobadifard, S. Mohebbi, Novel nanomagnetic Ag/β-Ag_2WO_4/$CoFe_2O_4$ as a highly efficient photocatalyst under visible light irradiation, New J. Chem., 42 (2018) 9530–9542.
[43] S. Huang, Y. Xu, M. Xie, H. Xu, M. He, J. Xia, L. Huang, H. Li, Synthesis of magnetic $CoFe_2O_4$/g-C_3N_4 composite and its enhancement of photocatalytic ability under visible-light, Colloids Surf. A, (2015) 93287126. doi: http://dx.doi.org/10.1016/j.colsurfa.2015.03.035
[44] Y. Li, L. Li, J. Hu, L. Yan, Spray pyrolysis synthesis of $MnFe_2O_4$/SnO_2 yolk/shell composites for magnetically recyclable photocatalyst, Mater. Lett., 199 (2017) 135–138.
[45] W. Wu, S. Zhang, F. Ren, X. Xiao, J. Zhou, C. Jiang, Controlled synthesis of magnetic iron oxides@SnO_2 quasi-hollow core–shell heterostructures: formation mechanism, and enhanced photocatalytic activity, Nanoscale, 3 (2011) 4676–4684.
[46] C. Karunakaran, S. Sakthiraadha, P. Gomathisankar, P. Vinayagamoorthy, Fe_3O_4/SnO_2 nanocomposite: hydrothermal and sonochemical synthesis, characterization, and visible-light photocatalytic and bactericidal activities, Powder Technol., 246 (2013) 635–642.
[47] I. Arshadnia, M. Movahedi, N. Rasouli, $SnFe_2O_4$/SnO_2/PANI magnetically separable photocatalyst for decolorization of two dye mixture in aqueous solution, Surf. Interfaces, 8 (2017) 91–96.
[48] T.V.K. Karthik, A. Maldonado, M. de la L. Olvera, Synthesis of Tin Oxide Powders by Homogeneous Precipitation. Structural and Morphological Characterization, 9th International Conference on Electrical Engineering, Computing Science and Automatic Control (CCE), Mexico City, 26–28 Sept. 2012, pp. 1–7. doi: 10.1109/ICEEE.2012.6421145
[49] B.M. Babić, S.K. Milonjić, M.J. Polovina, B.V. Kaludierović, Point of zero charge and intrinsic equilibrium constants of activated carbon cloth, Carbon, 37 (1999) 477–481.
[50] S.K. Milonjić, A.L. Ruvarac, M.V. Šušić, The heat of immersion of natural magnetite in aqueous solutions, Thermochim. Acta, 11 (1975) 261–266.
[51] E. Abroushan, S. Farhadi, A. Zabardasti, Ag_3PO_4/$CoFe_2O_4$ magnetic nanocomposite: synthesis, characterization and applications in catalytic reduction of nitrophenols and sunlight-assisted photocatalytic degradation of organic dye pollutants, RSC Adv., 7 (2017) 18293–18304.
[52] N. Adeela, K. Maaz, U. Khan, S. Karim, A. Nisar, M. Ahmad, G. Ali, X.F. Han, J.L. Duan, J. Liu, Influence of manganese substitution on structural and magnetic properties of $CoFe_2O_4$ nanoparticles, J. Alloys Compd., 639 (2015) 533–540.
[53] E.A. Davis, N.F. Mott, Conduction in non-crystalline systems V. Conductivity, optical absorption and photoconductivity in amorphous semiconductors, Philos. Mag., 22 (1970) 903–922.
[54] E. Sanchez, T. Lopez, Effect of the preparation method on the band gap of titania and Pt-titania sol-gel materials, Mater. Lett., 25 (1995) 271–275.
[55] F. Jahan, M.H. Islan, B.E. Smith, Band-gap and refractive-index determination of Mo-black coatings using several techniques, Sol. Energy Mater. Sol. Cells, 37 (1995) 283–293.
[56] L.G. Devi, M. Srinivas, Hydrothermal synthesis of reduced graphene oxide-$CoFe_2O_4$ heteroarchitecture for high visible light photocatalytic activity: exploration of efficiency, stability and mechanistic pathways, J. Environ. Chem. Eng., 5 (2017) 3243–3255.
[57] M. Thommes, K. Kaneko, A.V. Neimark, J.P. Olivier, F. Rodriguez-Reinoso, J. Rouquerol, K.S.W. Sing, Physisorption of gases, with special reference to the evaluation of surface area and pore size distribution (IUPAC Technical Report), Pure Appl. Chem., 87 (2015) 1051–1069.
[58] B.-H. Chen, W. Liu, A. Li, Y.-J. Liu, Z.-S. Chao, A simple and convenient approach for preparing core–shell-like silica@nickel species nanoparticles: highly efficient and stable catalyst for the dehydrogenation of 1,2-cyclohexanediol to catechol, Dalton Trans., 44 (2015) 1023–1038.
[59] G. Leofanti, M. Padovan, G. Tozzola, B. Venturelli, Surface area and pore texture of catalysts, Catal. Today, 41 (1998) 207–219.
[60] N.M. Flores, U. Pal, R. Galeazzi, A. Sandoval, Effects of morphology, surface area, and defect content on the photocatalytic dye degradation performance of ZnO nanostructures, RSC Adv., 4 (2014) 41099.
[61] P. Velusamy, G. Lakshmi, Enhanced photocatalytic performance of (ZnO/CeO_2)-β-CD system for the effective decolorization of rhodamine B under UV light irradiation, Appl. Water Sci., 7 (2017) 4025–4036.
[62] E. Tombácz, pH-dependent surface charging of metal oxides, Period. Polytech. Chem. Eng., 53 (2009) 77–86.
[63] C.C. Chen, C.S. Lu, Y.C. Chungb, J.L. Jan, UV light induced photodegradation of malachite green on TiO_2 nanoparticles, J. Hazard. Mater., 141 (2007) 520–528.
[64] S. Guo, G. Zhang, Y. Guo, J.C. Yu, Graphene oxide-Fe_2O_3 hybrid material as highly efficient heterogeneous catalyst for degradation of organic contaminants, Carbon, 60 (2013) 437–444.
[65] X. Yong, M.A.A. Schoonen, The absolute energy positions of conduction and valence bands of selected semiconducting minerals, Am. Mineral., 85 (2000) 543–556.